New insight on crystal and spot development in hard and extra hard cheeses: association of spots with incomplete aggregation of curd granules

SCHOLARONE™
Manuscripts

ScholarOne support: (434) 964 4100

1   <div align="center">**INTERPRETATIVE SUMMARY**</div>

2   **New insight on crystal and spot development in hard and extra hard cheeses: association of**

3   **spots with incomplete aggregation of curd granules**

4   **D'Incecco**

5   The study was carried out with a multidisciplinary approach, using techniques such as confocal,

6   Raman and electron microscopy, to shed light on the phenomenon of speck and spot blowing in

7   hard cheese. The obtained information on structure and chemical composition of these particles,

8   allowed us to formulate an original theory for their genesis. Furthermore, these results provide

9   useful information to be applied in cheese making technology in order to contain the incidence of

10   the speck and spot phenomenon.

11

12   **RUNNING HEAD: CRYSTALS AND SPOTS IN HARD AND EXTRA HARD CHEESES**

13   **New insight on crystal and spot development in hard and extra hard cheeses: association of**

14   **spots with incomplete aggregation of curd granules**

15   **P. D'Incecco,*[1] S. Limbo,* F. Faoro,[†] J. Hogenboom,* V. Rosi,* S. Morandi,[‡] L. Pellegrino***

16

17   * Department of Food Environmental and Nutritional Sciences, State University of Milan, 20133

18   Milan, Italy.

19

20   [†] Department of Agricultural and Environmental Sciences - Production, Landscape, Agroenergy,

21   State University of Milan, 20133 Milan, Italy.

22

23   [‡] Institute of Sciences of Food Production–Italian National Research Council, 20133 Milan, Italy.

24

25   [1]Corresponding author: P. D'Incecco

26   Department of Food, Environmental and Nutritional Sciences, University of Milan, Via Celoria 2,

27   20133 Milan, Italy

28   Telephone: (+39) 0250316679

29   Fax: (+39) 0250316672

30   E-mail: paolo.dincecco@unimi.it

31

32   **ABSTRACT**

33   Chemical composition and structure of different types of macro- (specks, spots) and micro particles

34   (microcrystals) present in hard and extra hard cheeses were investigated. Light microscopy revealed

35   that the small, hard specks had the structure of crystalline tyrosine, as confirmed by amino acid

36   analysis. Spots showed a complex structure, including several curd granules, cavities, and

37   microcrystals, and were delimited by a dense protein layer. Spots contained less moisture and ash

38   than the adjacent cheese area, and more protein, including significantly higher contents of valine,

39   methionine, isoleucine, leucine, tyrosine and phenylalanine. Microcrystals were observed by light

40   and electron microscopy and analysed by confocal micro Raman. Among others, calcium phosphate

41   crystals appeared to consist of a central star-shaped structure immersed in a matrix of free fatty

42   acids besides leucine and phenylalanine, in free form or in small peptides. A hypothetical

43   mechanism for the formation of these structures has been formulated.

44

45   **Keywords**: hard and extra hard cheeses, cheese ultrastructure, calcium phosphate crystal, free

46   amino acids, electron microscopy

47

48 **INTRODUCTION**

49 Hard and Extra-Hard are attributes used to define cheeses having a firm and brittle body texture

50 (Codex Alimentarius, 1978). Hard and extra-hard cheeses share low moisture content, close

51 structure, and a long ripening period. During ripening, many chemical, biochemical and

52 microbiological phenomena take place. The biochemical changes are very important for the

53 development of the flavour and texture of these cheeses and are characteristic of the different

54 varieties. Proteolysis is the most relevant among the biochemical phenomena due to its complexity

55 and final impact on the cheese taste. In fact, casein breakdown progressively brings to large and

56 medium peptides, then to small peptides and free amino acids (FAA). Since FAA are rather stable,

57 they tend to accumulate with the ripening time and may reach up to 20-24% on cheese protein basis

58 in 10-12 months old extra-hard cheeses (Masotti et al., 2010). Proteinases and peptidases that

59 catalyse proteolysis in cheese originate from different sources, namely milk, rennet, starter and non-

60 starter lactic acid bacteria (LAB). LAB have complex enzyme patterns that release peptides and

61 amino acids from the proteins into the cheese environment to satisfy their own nutritional

62 requirements (Gatti et al., 2014). After vat processing, the loss of water, diffusion of salt, and

63 formation of soluble molecules, such as FAA and lactate, are factors concurring to the increase of

64 solute concentration and concomitant decrease of water activity (a_w) in cheese throughout the whole

65 ripening period. Beside these main events, minor changes contribute to lower the water activity in

66 cheese, like changes in water binding by new carboxylic and amino groups formed on protein

67 hydrolysis (McSweeney, 2004). The moisture content and a_w are strongly correlated in cheese

68 throughout ripening (Marcos, 1993).

69 The increasing solute (salt, ions, FAA) concentration in cheese water phase may give rise to

70 aggregation and crystallization phenomena that result in different types of structures observed by

71 some authors in the interior and on the surface of different cheese varieties (Bianchi et al., 1974;

72 Agarwal et al., 2006; Tansman et al., 2015). Although earliest studies date back to the 1900s

4

73 (Babcock et al., 1903; Tuckey et al., 1938), a clear and unambiguous characterization of these

74 structures has not been achieved yet. Moreover, an univocal association between the terminology

75 (e.g. crystals, specks, dots, granules, spots, pearls) and the appearance of these structures is still

76 lacking.

77 In long ripened extra-hard cheeses, having a thick dry rind, these structures develop inside the

78 cheese becoming visible when the wheel is cut. Typically, two different types of structures visible

79 to the naked eye can be observed, referred to as specks and spots in this article. Specks look bright

80 white and firmer against the cheese matrix, and are usually smaller than 2-3 mm. Consumers

81 (cheese lovers) appreciate the crispness of the specks while chewing the cheese and their

82 contribution to the overall cheese taste. Previous studies about specks reported them to contain

83 clusters of tyrosine, cysteine as well as other FAA, calcium lactate and magnesium (Shock et al.

84 1948) or tyrosine and phenylalanine (Giolitti and Mascherpa, 1970). More recently, Bottazzi et al.,

85 (1994) and Tansman et al., (2015) converged on identifying them as tyrosine crystals in extra hard

86 cheeses.

87 Spots are spherical and paler than the cheese, and can grow up to 4-5 mm. They appear to be

88 amorphous and firmer with respect to the surrounding cheese matrix, and become visible after 10-

89 12 months of ripening. Spots can become so numerous and flashy that may influence the visual

90 appeal of the cheese. Spots have been very little studied, moreover without achieving consistent

91 results (Giolitti and Mascherpa, 1970; Bianchi et al., 1974; Tansman et al., 2015).

92 Besides specks and spots, extra-hard cheeses contain microscopic crystals, mostly investigated in

93 Cheddar cheese. However, some authors generically referred to crystals, without distinguishing

94 between the microscopic ones and those visible to the naked eye (Kalab, 1980; Bottazzi et al., 1982;

95 Washam et al., 1985; Bottazzi et al., 1994).

96 The aim of the present work was to shed light on the nature and origin of specks, spots and

97 microscopic crystals in extra-hard cheeses by a multidisciplinary approach. Due to the effectiveness

98 in cheese structure studies (Ong et al., 2010; Schrader et al., 2012; D'Incecco et al., 2015), various

5

99   microscopy techniques and different dyes (light and fluorescence, confocal, confocal micro Raman

100   and transmission electron microscopy) were used in combination with chemical data to achieve an

101   unambiguous characterization of these particles in cheese. Our ultimate goal was to formulate an

102   hypothesis on the origin of these structures as they appear in hard and extra-hard cheeses. This

103   knowledge will contribute useful information to understanding the bioavailability of selected

104   minerals and nutrients in cheese. Furthermore, this knowledge could provide insights into the nature

105   of these structures that might lead to new manufacturing strategies to control the formation of spots

106   in commercial cheeses.

107   **MATERIALS AND METHODS**

108   **Cheese samples and collection of specks and spots.** Eleven extra-hard cheeses, ripened for 18-20

109   months, were kindly provided by two dairies producing Grana Padano (7 cheeses) and Parmigiano-

110   Reggiano (4 cheeses) respectively. Specks were harvested from the cheese using a pin, while spots

111   were collected from the cheese using a spatula and then gently brushed to remove the cheese matrix

112   on the surface. Specks and spots were separately collected from individual cheese samples in a

113   sufficient amount (20-22 g) to conduct all the analyses. Equivalent cheese amount was taken from

114   the portion (0.5-cm thick) immediately surrounding the single spot, as shown in Figure 1, as used as

115   a term of reference. When necessary, a slice representative of the whole cheese was taken as well.

116   Additional cheese portions were taken as required for microscopy investigations with various

117   techniques. In particular, 20 spots of different size and taken from different cheeses were observed

118   for their structural characterization.

119   **Chemicals.**

120   Glutaraldehyde, paraformaldehyde, cacodylate buffer, and osmium tetroxide were purchased from

121   Agar Scientific (Stansted, UK). Toluidine blue, rhodamine and single amino acids were purchased

122   from Sigma Aldrich (Milan, Italy). Ninhydrin was purchased from Biochrom Ltd (Cambridge, UK).

123   Water purified with Milli-Q system (Millipore Corp., Bedford, MA) was used.

124   **Composition analyses.**

125   The ISO Standard methods for cheese were used to determine the content of protein (ISO

126   27871:2011), fat (ISO 1735:2004), ash (ISO 5545:2008) and moisture (ISO5534:2004),

127   respectively. Content of calcium and phosphorus were determined by ICP-MS spectrometer

128   (Agilent Technologies, Milan, Italy).

129   The pattern of FAA was determined on the various cheese portions (including pecks and spots)

130   using the method described by Masotti et al. (2010). Briefly, the cheese portion was solubilized

131   with sodium citrate, homogenized and deproteinized with sulphosalicilic acid. The extract was

132   diluted (1:1) with lithium citrate buffer at pH 2.2, filtered and analysed by ion exchange

133   chromatography. The chromatographic separation was carried out on a Biochrom 30+ (Biochrom

134   Ltd, Cambridge, UK) amino acid analyser operated under the conditions provided by the

135   manufacturer. These employ an eight-step elution program with lithium citrate buffers of increasing

136   pH and ionic strength, post-column derivatisation with ninhydrin, and detection at 440 and 570 nm.

137   The quantification was carried out using four-level calibration lines of the 21 amino acids in the

138   range 0.75-22.5 mg/L and using norleucine (Sigma Aldrich) as an internal standard. Repeatability

139   values of ISO Standard 13903:2005 were fulfilled.

140   **Amino acid diffusion trial**.

141   To confirm the different diffusivity of individual FAA within the cheese, 0.3 mL of an aqueous

142   FAA solution having three times the concentration of the cheese water phase was injected into the

143   core of a spot-free cheese portion (a disk of 10 g) using a microsyringe. The cheese portion was

144   kept in a forced-ventilation thermostatic oven at 18 °C for 18 days and then sampled as described in

145   the Results. The FAA pattern and the moisture content were determined in each sampled portion.

146   **Light and Confocal Microscopy.**

147   Specimens for light and fluorescence microscopy observations were thin sections obtained from

148   resin-embedded cheese samples prepared as below described for transmission electron microscopy

149   (TEM). Thin sections (4-5 per sample) were directly dried on the microscope slide, stained and

150   subsequently washed. Two different staining were performed, (i) toluidine blue (1% in water, w/v)

7

151 for 5 min at room temperature, to visualize the overall protein structure by light microscopy, and (ii)

152 rhodamine B (0.5% in water, w/v) for 5 min at room temperature. In the latter case, the sample was

153 examined by a Hg lamp, with the following filters: excitation wavelength = 570 nm, emission

154 wavelength = 590 nm. In addition a 5-cm cube of cheese was immersed in ninhydrin solution for 1

155 h and then cut with a blade until a thin section containing a spot was obtained. All samples were

156 examined with an Olympus BX optical microscope (Tokyo, Japan) equipped with Nomarski

157 interference contrast and QImaging Retiga camera (Surrey, BC, Canada). Specimens for confocal

158 microscopy observations were cryo-sectioned by a CM1950 cryostat (Leica, Germany) and stained

159 directly onto the microscope slide with fast green (0.1 % in water, w/v). Sections were examined

160 with a Video confocal microscope, Nikon Vico (Tokyo, Japan).

161 **Transmission Electron Microscopy.**

162 Cubes of cheese (1 mm edge length) were fixed in a mixture (w/v) of glutaraldehyde 3% and

163 paraformaldehyde 2% in cacodylate buffer for 2 h at 4 °C, then washed with cacodylate buffer for 1

164 h and post-fixed in osmium tetroxide (1% in water, w/v) for 2 h. After the dehydration in an ethanol

165 series, the samples were embedded in London Resin White ™ resin and cured at 60 °C for 24 h.

166 Ultrathin sections (50 to 60 nm thick) were stained with uranyl acetate and lead citrate and

167 examined with a Philips E208 transmission electron microscope (Aachen, Germany).

168 **Confocal Micro Raman.**

169 The Raman spectral data were collected in the range from 3200 to 200/cm Raman shift using a

170 confocal DXR Raman Microscope (Thermo Scientific, Waltham, MA, USA). An Olympus 50X

171 objective (numerical aperture 0.75) with a 50 μm confocal pinhole was used to collect the Raman

172 signal directly from a flat area of the sample (cut using a sharp knife) with a spatial resolution lower

173 than 1 μm, without any preparation of the sample. A laser with an excitation wavelength of 780 nm

174 with a low energy power (5-10 mW) to avoid overheating and a 400 lines/mm grating was used to

175 record Raman spectra over the focalized area. A photobleaching time equal to 1 min was set up. For

176 the specks, spectra were collected individually while for the microcrystals a selected area was

8

177   analysed collecting around 70 spectra over the entire surface, using 10 μm as the interval between

178   positions. In particular, each sample was placed on an automated x,y mapping stage and Raman

179   spectra were obtained at different points of the selected surface, by moving it under the microscope

180   objective. Autofocus at each map point was applied. Omnic Atlμs software (Thermo Fisher

181   Scientific, Madison, WI, USA) was used to obtain Raman spectra, perform spectrometer operations

182   and process data. All spectra were corrected for background contributions and an automated

183   subtraction of cosmic ray peaks was employed.

184   **Statistical analysis**

185   Statistical treatment of data was performed by means of SPSS Win 12.0 program (SPSS Inc.,

186   Chicago, IL, USA). Data were analysed by Student's t-test and one way Anova. A $P<0.05$ was

187   assumed as significance limit.

188   **RESULTS**

189   **Speck characterization.** Attempts to obtain a section of specks or to embed them in resin failed

190   because they were too hard and packed. In contrast, specks *in toto* could be directly observed by

191   light microscopy after isolation by cheese and showed the characteristic structure of crystalline

192   tyrosine (Figure 2). The FAA pattern (Figure 2) indicated that specks were indeed tyrosine crystals

193   of > 95% purity. The peak of ammonia in the chromatogram derived from the elution buffers and

194   thus was ignored in purity calculation. The Raman spectrum also confirmed the nature of the

195   specks: the doublet Raman bands at 828 and 848/cm due to the Fermi resonance between ring

196   fundamental and overtone were strongly evident, as was the ring-O stretching vibration located at

197   1263/cm (Culka et al., 2010). Also the highly resolved bands found in the finger print region (1614-

198   250/cm) were associated to the signals collected for the solid and pure (98-99%) crystalline form of

199   L-tyrosine (spectrum not shown).

200   **Spot characterization.**

201   Spot structure was firstly examined by light microscopy. A cheese portion was immersed in the

202   protein-staining solution (ninhydrin) and then sectioned up to reveal a spot inside which appeared

203 surrounded by an highly dense layer (Figure 3, arrowhead) that impaired staining permeation inside.

204 However, some stain could permeate through preferential micro pathways (junctions, indicated by

205 arrows in Figure 3), making the structure visible. Thin sections of resin-embedded spots, stained

206 with toluidine blue, gave more insight of the inner structure (Figure 4a). The spot appeared as made

207 of several curd particles having clean-cut irregular shapes and size up to 0.5 mm. The darker lines,

208 corresponding to the junctions among curd particles, were richer in protein than the particle body.

209 Several openings, including a large hole collecting the junctions, were visible in the section (Figure

210 4b). Although the cheese around the spot showed the same composite structure (not shown), large

211 cavities were observed only inside spots. With respect to the curd particles, the junctions appeared

212 as thick protein strings almost free of fat (Figure 4c) and rich in microcrystals (arrows).

213 Microcrystals were also observed in the cheese matrix outside the spot, as further discussed.

214 The ultrastructure of the spot, examined by TEM, proved to be remarkably different compared to

215 that of the surrounding cheese (Figure 5). In particular, the interface between protein (Figure 5, in

216 grey) and fat (in white) was more irregular and fringed by crystal-like particles (Figure 5a) in

217 respect with the cheese surrounding the spot (Figure 5b).

218 The chemical composition of the spots was compared to that of the cheese portion just around them

219 and to that of the whole cheese. Five different cheeses were individually analysed (Table 1). Spots

220 proved to be significantly richer in protein ($p<0.00$) and poorer in moisture ($p<0.00$) and ash

221 ($p<0.00$) with respect to the surrounding cheese portion, which did not differ from the whole

222 cheese. Fat content was not different ($p<0.17$). The contents of both calcium and phosphorus were

223 10% lower in the spot than in the cheese, with a Ca/P molar ratio of 1 in both zones (not shown).

224 The protein fraction was characterized by capillary zone electrophoresis as described in our

225 previous work (Masotti et al., 2010). No difference could be evidenced, neither in casein nor in

226 peptide patterns, between the spots and the rest of the cheese (not shown), indicating that the

227 primary proteolysis had proceeded to the same extent within and outside the spot. On the contrary,

228 significant differences were found in the FAA patterns of the two zones.

10

229   In order to compare data of cheese portions (i.e. spots and surrounding cheese) having different

230   moisture contents, and considering that FAA are soluble molecules, values were expressed on the

231   respective moisture content. Furthermore, data from both Grana Padano and Parmigiano-Reggiano

232   were pooled to increase statistical significance. In particular, spots contained significantly higher

233   amounts (from 4 to 12 times) of six FAA, i.e. valine ($p<0.00$), methionine ($p<0.00$), isoleucine

234   ($p<0.00$), leucine ($p<0.00$), tyrosine ($p<0.00$) and phenylalanine ($p<0.00$) (Figure 6). It is worthy of

235   remark that the content of the other FAA was the same as in the cheese portion around the spot.

236   Nevertheless, this last portion had the usual FAA pattern we observed for the two target cheeses in

237   previous studies (Cattaneo et al., 2008; Masotti et al., 2010). To achieve direct confirmation of such

238   a different composition in individual FAA within the cheese, a simple experiment was carried out.

239   A water solution having the approximate concentration of FAA in cheese water phase was injected

240   into a spot-free cheese slice. After a resting time suitable to allow diffusion of the solution, the

241   cheese was sampled taking three distinct portions: one circular, corresponding to the injection point

242   (mimicking the spot), and two concentric rings around it, as shown in Figure 7 (inset). Despite of

243   the approximate experimental conditions and sampling procedure, the obtained data confirmed that

244   the same six FAA were retained in the zone where the mixture was injected, while the others

245   diffused to the surrounding portions largely reaching an equilibrium (Figure 7).

246   **Microscopic crystals.**

247   Microscopic crystals were investigated through various microscopy techniques. Observations by

248   fluorescence microscopy of cheese semi-thin sections, after resin embedding and staining with

249   rhodamine B, allowed to see a huge number of microscopic crystals in bright red (Figure 8a).

250   Confocal microscopy showed that crystals had different shapes, i.e. circular, oval or kidney-shaped,

251   and their core was not fluorescent, indicating a different composition in respect to the peripheral

252   zone (Figure 8b). The number of crystals ranged from 30 to 100 crystals/mm^2 in 18-20 months

253   ripened cheeses and apparently was not different between cheese and inside spots. Crystals with the

254   same structure were detected in younger (three and six months of ripening) extra hard cheeses,

255   although in a lower amount (not shown).

256   Microscopic crystals observed by TEM showed a complex ultrastructure (Figure 8c). Three main

257   zones could be outlined: (i) a central star-shaped crystal, (ii) an intermediate zone and (iii) a

258   peripheral compact shell at the interface with the protein matrix. Figures 8d shows both the external

259   shell and the intermediate zone to be constituted by fibrils with prismatic morphology, radially

260   ordered and packed around the central crystal.

261   Confocal Raman microscopy was used to obtain information on the chemical composition since this

262   technique does not require any sample preparation. Area maps of the crystals, detected both inside

263   and outside the spot, confirmed the presence of distinct regions, as observed by TEM. Spectra of the

264   central star shaped crystal matched the calcium phosphate spectrum, dominated by the very strong

265   band at 986/cm and the medium band at 878/cm (Figure 9) that derived from the symmetric

266   stretching mode of the phosphate group (Sauer et al., 1994). The band at 1081/cm corresponded to

267   the stretching vibration (υ_3) of PO_4^{3-}, while the band at 588/cm to the P-O and O-P-O stretching and

268   bending modes (υ_4) of the same group. In calcium phosphate crystals, the minerals can be identified

269   by the position and shape of the main bands. Raman shifts and assignment for some calcium

270   phosphate minerals were studied by Koutsopoulos (2002). The Savitsky-Golay second derivative of

271   the spectra highlighted the presence of other weak bands attributable to the dibasic calcium

272   phosphate dehydrate form. No calcium phosphate was detected in other parts of the complex crystal

273   structure. In fact, in the outer zone, appearing as a dark area in the optical magnification used for

274   the Raman acquisition, spectra presented bands that arose from both free fatty acids and proteins

275   (Figure 10a). The spatial distribution of fatty acid/protein with respect the calcium phosphate within

276   the crystal area is shown in Figure 10b (in blue). It is evident that the crystal is immersed in the

277   cheese matrix. A deeper analysis of the spectra of this portion provided a major characterization of

278   the protein structure contribution. Usually, the amide I and III peaks in a protein are less sharply

279   resolved if compared with the signals of small peptides (Jenkins et al., 2005). In other words,

280 Raman spectral signatures of the single amino acids are retained in the peptide or protein, being

281 largely derived from their side chain or backbone. The higher the resolution and intensity of the

282 bands in a complex spectrum, the more probable the contribution of amino acids and/or small

283 peptides. Thus, in the original spectrum collected from the cheese matrix around the phosphate

284 crystal, some peculiar bands of amino acids were evident. In particular, a spectral subtraction of an

285 unsaturated free fatty acid spectrum (considered as a background) from the original spectrum of the

286 external region returned the profile of leucine (match higher than 60% with the pure spectrum of L-

287 leucine) and phenylalanine (match equal to 53% with the pure spectrum of L-phenylalanine).

288 Leucine was mainly characterized by the bands at 1237/cm due to the twisting of CH_2, and by the

289 bands at 1187 and 1132/cm due to the rocking of NH_3^+, whilst phenylalanine showed a very intense

290 band around 1000/cm. These results indicated that the protein component around the crystal was

291 mainly due to these two amino acids, present in free form or in small peptides.

292 Other crystalline structures were randomly detected within the cheese and analysed by means of

293 micro Raman spectroscopy. Only calcium carbonate crystals were identified so far. They appeared

294 spheroidal in shape and translucent: the peaks at 1083, 1410, 713 and 284/cm confirmed their

295 nature (Tlili et al., 2001) (data not shown). The presence of calcium carbonate in cheese seems to be

296 attributable to the microbial metabolism that produces CO_2 (Gaucheron et al. 1999).

DISCUSSION

Speck characterization

299 By evaluating the confocal micro Raman spectrum and FAA composition of specks we obtained a

300 tyrosine purity >95% confirming previous reports indicating the presence of this amino acid in

301 these structures (Bottazzi et al., 1994; Tansman et al., 2015). Free tyrosine concentration increases

302 in the whole cheese throughout the ripening process, like for all other FAA (Pellegrino et al., 1997).

303 In our samples of Grana Padano and Parmigiano-Reggiano, free tyrosine concentration was

304 approximately 0.8 g / 100 g of water phase (Figure 6), i.e. about ten times higher than its water

305 solubility at room temperature (Grosse Daldrup et al., 2010). Therefore, formation of crystals

13

306 spread within the cheese would suggest that progress of proteolysis is not homogeneous in the

307 matrix thus leading to FAA accumulation, including tyrosine, preferentially into micro openings

308 until saturation. Furthermore, we have obtained by light microscopy further structural details of

309 tyrosine crystals from cheese (Figure 2), showing that the former reported description (Tansman et

310 al., 2015) is due to micro spike of the crystalized amino acid. When observed by atomic force

311 microscopy in protein hydrolysates (McPherson et al., 2012), tyrosine crystals appeared to be

312 covered by a stable layer of 3-nm particles, likely represented by micellar arrangement of small

313 peptides present in the medium and able to prevent re-solubilisation of crystals once formed.

314 Considered the remarkable content of peptides in ripened cheeses, this aspect would be worthy of

315 investigation.

Spot characterization

317 Contrary to the hard specks, spots were easily resin embedded and cut into thin sections that

318 allowed a deeper characterization by various microscopy techniques. Previous studies on spots in

319 cheese did not investigate their structure and ultrastructure (Giolitti and Mascherpa, 1970; Bianchi

320 et al. 1974; Tansman et al., 2015). Unexpectedly, when the cheese was directly stained with

321 ninhydrin and observed by light microscopy, the original grains of curd were still visible. During

322 cheese manufacturing, curd grains (20-50 mm), obtained by cutting the rennet gel, are let in hot

323 whey for 50-60 min to settle and aggregate at the bottom of the vat. Further fusing and shrinking of

324 curd grains are induced by the subsequent acidification of the cheese loaf when kept in mould for

325 48 hours. Since Grana Padano and Parmigiano-Reggiano loaves are not pressed, high temperature

326 and low pH (5.2-5.3) play the major role in promoting whey draining (Pellegrino et al., 1997) and

327 the tight aggregation of curd grains. However, as said above, these grains appeared as separate units

328 even several months later. The junctions between contiguous grains are low in fat because many fat

329 globules escape the protein network at the surface of the grains before they stick together. For those

330 grains having either irregular shape or different size their aggregation during settling forms an

331 internal hole, connected with several openings and radial junctions. This pattern was frequently

14

332 observed within the spots (Figure 3b). In the young cheese, even before the spot formation, these

333 hollow cavities likely represent preferential zones where whey stagnates and entrapped bacterial

334 cells find substrates for growth (Le Boucher et al., 2016). Growth of bacterial colonies as affected

335 by local concentration of substrates in cheese is receiving increasing attention (Silva et al., 2013;

336 Jeanson et al., 2015). Although no intact bacterial cells were detected by TEM in cavities within the

337 spot, as well as in the surrounding cheese, likely due to the prolonged ripening process, an indirect,

338 preliminary confirmation of this hypothesis came out by measuring the amount of total DNA

339 extracted from the spot and the surrounding cheese following the procedure of (Cremonesi et al.,

340 2007). In fact, DNA amount was more than three times higher in the spots than in the surrounding

341 cheese (72.94 μg *vs* 22.41 μg/mg).

342 Spots proved to be significantly more dry, with respect to the surrounding cheese portion, and to

343 contain more protein and less ash (Table 1), confirming the data reported by Tansman et al. (2015).

344 In addition, we showed the cheese portion just around the spot had the same chemical composition

345 as the rest of the cheese, confirming that the spot is a fully isolated unit. The dense layer we

346 observed around it by light microscopy is likely responsible for this (Figure 3, arrowhead). Overall,

347 these findings point to a migration of whey, with consequent draining of solutes, occurring locally

348 within the cheese where the spot would originate later.

349 Spots were also reported to have a different FAA composition compared to the whole cheese.

350 Bianchi et al. (1974) found spots in 18- and 25-month ripened Grana Padano cheeses to contain

351 (g/100 g): leucine (9.86), isoleucine (4.96), methionine (1.64), valine (1.52), glutamic acid (1.84),

352 and asparagine (1.63), as dominant FAA. However, these authors did not notice that the last two

353 FAA were equally abundant in the whole cheese. Recently, Tansman et al. (2015) detected only 1%

354 of free leucine in spots from a 24-month old Parmigiano-Reggiano cheese but they did not give

355 explanation for the discrepancy of this result with those of literature. We obtained FAA data similar

356 to those of Bianchi et al. (1974), however we put forward a different interpretation. The key to

357 understand the genesis of the spot relays in the chemical properties of the different FAA present in

15

358 the spot and in the cheese regardless of their concentration. In fact, the six FAA we detected at

359 much higher levels in the spot (i.e. leucine, isoleucine, methionine, valine, phenylalanine and

360 tyrosine) (Figure 6) are all hydrophobic because of either the aromatic or branched chain structure,

361 and thus insoluble in the water phase of cheese. This shared FAA characteristic leads us to

362 hypothesise that local water movements are responsible for their different distribution and,

363 consequently, for the spot blowing in hard and extra hard cheeses. This hypothesis was confirmed

364 by our experiment mimicking the migration of FAA within the cheese.

365 As already mentioned, in young cheese the cavities in which the residual whey stagnates could be

366 the sites where bacterial colonies develop. During cheese ripening, the water phase in these sites

367 becomes more concentrated in solutes due to lactic acid bacteria metabolism and, at a later stage, to

368 cell lysis. Progressively, the water phase migrates through the curd grain junctions, dragging solutes

369 including, preferentially, polar FAA over the hydrophobic ones. Consequently, less water soluble

370 molecules concentrate in a restricted area, that evolves into a spot, from which water moves away

371 radially (Figure 7) dragging away also salts. For this reason, many crystals were visible in the

372 junctions (Figure 4c).

Microscopic crystal characterization

374 Microcrystals appeared to be spread within the whole cheese. Among these crystals we have up to

375 now identified calcium phosphate by micro Raman, directly on the cheese, without any sample

376 preparation. The central star shaped crystals observed by TEM (Figure 8c) were clearly assigned to

377 selected types of calcium phosphate. Gaucheron et al. (1999) demonstrated that the supersaturation

378 of calcium phosphate salts increases strongly during cheese ripening due to the rise of pH,

379 explaining the salt precipitation. Unfortunately, the few references that discuss crystals

380 ultrastructure in cheese give no indication about the nature of the calcium phosphate. In our study,

381 the micro Raman analysis produced sufficient information about their morphological features and

382 complex ultrastructure. In fact, this technique allowed to evidence for the first time that the

383 fibrillary layer surrounding the central crystal contains leucine and, to a lower amount,

16

384   phenylalanine. These hydrophobic amino acids are reported to limit growth of calcium phosphate

385   crystals due to their absorption on the crystal surface that blocks the active growth sites (Dalas et

386   al., 2008). Although calcium lactate could form in cheese, due to lactic acid fermentation, the

387   chelation of calcium by the phosphates should greatly prevail (Heertje et al., 1981), in agreement

388   with the relevant number of calcium phosphate crystals we detected. Arkwall et al. (2006) reported

389   that calcium lactate crystals only form when pH is higher than 5.1. We could not find calcium

390   lactate crystals, although we cannot exclude their presence in extra hard cheeses, as different

391   unidentified crystalline structures were observed by TEM. Some researcher detected calcium lactate

392   crystals in cheeses other than Grana Padano and Parmigiano-Reggiano (Washam et al., 1982;

393   Tansman et al., 2014), whereas only Bottazzi et al. (1982) detected them in 14-month ripened Grana

394   cheese indicating their low incidence, i.e. 2-3 per square mm.

395   Presence of leucine crystals is likely within the spot where free leucine showed a concentration in

396   the water phase ten times higher than in the cheese (Figure 6). Crystalline leucine was also detected

397   by Tansman et al. (2015) in pearls collected from Parmigiano-Reggiano cheese.

CONCLUSIONS

399   In conclusion, combining the background knowledge about extra-hard cheese manufacturing and

400   ripening with the new information about composition and structure of spots achieved in this study,

401   we can hypothesize an incomplete aggregation of curd granules and a consequent local whey

402   stagnation to be at the origin of spot development. Growth and lysis of bacterial cells entrapped in

403   these micro cavities influence both metabolite availability and micro environmental conditions, that

404   in turn regulate diffusion and crystallization of solutes locally. Therefore, all practices finalized to

405   the syneresis improvement, such as fine-tuning of temperature control and curd grain size, would

406   greatly reduce spot number and the occurrence of other confined phenomena.

REFERENCES

408   Agarwal, S., J. R. Powers, B. G. Swanson, S. Chen, and S. Clark. 2006. Cheese pH, protein

409   concentration, and formation of calcium lactate crystals. J. Dairy Sci. 89: 4144-4155.

410

411   Agarwal, S., K. Sharma, B. G. Swanson, G. U. Yüksel, and S. Clark. 2006. Nonstarter lactic acid

412   bacteria biofilms and calcium lactate crystals in Cheddar cheese. J. Dairy Sci. 89: 1452–

413   1466.

414

415   Babcock, S. M., L. H. Russel, A. Vivian, and U. S. Baer. 1903. Condition affecting the

416   development of white specks in cold-curd cheese. Pages 180-183 in Wis. Agric. Expt. Sta.

417   19th Annu. Rep.

418

419   Bianchi, A.; G. Beretta, G. Caserio, and G. Giolitti. 1974. Amino acid composition of granules and

420   spots in Grana Padano cheeses. J. Dairy Sci. 57: 1504–1508.

421

422   Bottazzi, V., B. Battistotti, and F. Bianchi. 1982. The microscopic crystalline inclusions in Grana

423   cheese and their x-ray microanalysis. Milchwissenschaft Milk Sci. Internat. 37: 577–580.

424

425   Bottazzi, V., F. Lucchini, A. Rebecchi, and G. L. Scolari. 1994. I cristalli del formaggio grana

426   (Crystals present in Grana cheese). Sci. Tecn. Latt.-Cas. 45: 7–14.

427

428   Cattaneo, S., J. A. Hogenboom, F. Masotti, V. Rosi, L. Pellegrino, and P. Resmini. 2008. Grated

429   Grana Padano cheese: new hints on how to control quality and recognize imitations. Dairy

430   Sci. Technol. 88: 595-605.

431

432   Codex General Standard for Cheese. Codex Standard 283-1978.

433

434   Cremonesi, P., G. Perez, G. Pisoni, P. Moroni, S. Morandi, M. Luzzana, M. Brasca, and B.

435   Castiglioni. 2007. Detection of enterotoxigenic Staphylococcus aureus isolates in raw milk

436   cheese. Lett. Appl. Microbiol. 45: 586–591.

437

438   Culka, A., J. Jehlicka, and H. G. M. Edwards. 2010. Acquisition of Raman spectra of amino acids

439   using portable instruments: Outdoor measurements and comparison. Spectrochim. Acta A.

440   77: 978–983.

441

442   Dalas, E., P. Malkaj, Z. Vasileiou, and D. G. Kanellopoulou. 2008. The effect of Leucine on the

443   crystal growth of calcium phosphate. J. Mater. Sci.: Mater. Med. 19: 277-282.

444

445   D'Incecco, P., F. Faoro, T. Silvetti, K. Schrader, and L. Pellegrino. 2015. Mechanisms of

446   Clostridium tyrobutyricum removal through natural creaming of milk: A microscopy study.

447   J. Dairy Sci. 98: 5164-5172.

448

449   Gatti, M., B. Bottari, C. Lazzi, E. Neviani, and G. Mucchetti. 2014. Invited review: Microbial

450   evolution in raw-milk, long-ripened cheeses produced using undefined natural whey

451   starters. J. Dairy Sci. 97: 573-591.

452

453   Gaucheron, F., Y. Le Graet, F. Michel, V. Briard and M. Piot. Evolution of various salt

454   concentrations in the moisture and in the outer layer and centre of a model cheese during its

455   brining and storage in ammoniacal atmosphere. Lait. 79: 553-566.

456

457   Giolitti, G. and G. F. Mascherpa. 1970. La formazione di depositi di tirosina in formaggi a lunga

458   stagionatura. Ind. Latte. 6: 83-85.

459

460   Grosse Daldrup, J. B., C. Held, F. Ruether, G. Schembecker, and G. Sadowski. 2009. Measurement

461   and modeling solubility of aqueous multisolute amino-acid solutions. Ind. Eng. Chem. 49:

462   1395–1401.

463

464   Heertje, I., M. J. Boskamp, F. Van Kleef, and F. H. Gortemaker. 1981. The microstructure of

465   processed cheese. Neth. Milk Dairy J. 35, 177.

466

467   Jeanson, S., J. Floury, V. Gagnaire, S. Lortal, and A. Thierry. 2015. Bacterial colonies in solid

468   media and foods: a review on their growth and interactions with the micro-environment.

469   Front. Microbiol. 6: 1284.

470

471   Jenkins, A. L., R. A. Larsen, and T. B. Williams. 2005. Characterization of amino acids using

472   Raman spectroscopy. Spectrochim. Acta A. 61: 1585–1594.

473

474   Kaláb, M., J. Yun, and S. H. Yiu. 1987. Textural properties and microstructure of process cheese

475   food rework. Food Microbiol. 6: 181-192.

476

477   Koutsopoulos, S. 2002. Synthesis and characterization of hydroxyapatite crystals: a review study on

478   the analytical methods. J. Biomed. Mater. Res., 62: 600-612.

479

480   Le Boucher, C., V. Gagnaire, V. Briard-Bion, J. Jardin, M. B. Maillard, G. Dervilly-Pinel, B. Le

481   Bizec, S. Lortal, S. Jeanson, and A. Thierry. 2016. Spatial distribution of Lactococcus lactis

482   colonies modulates the production of major metabolites during the ripening of a model

483   cheese. Appl. Environ Microbiol. 82: 202–210.

484

485   Marcos, A. 1993. Water activity in cheese in relation to composition, stability and safety. Pages

486   439-469 in Cheese: Chemistry, Physics and Microbiology, Vol. 1, ed.; Fox. P. F.; Chapman

487   & Hall, London.

488

489   Masotti, F., J. A. Hogenboom, V. Rosi, I. De Noni, and L. Pellegrino. 2010. Proteolysis indices

490   related to cheese ripening and typicalness in PDO Grana Padano cheese. Int. Dairy J. 20:

491   352-359.

492

493   McPherson, A., S. B. Larson, and Y. G. Kuznetsov. 2012. Tyrosine Microcrystals Produced by

494   Digestion of Proteins with Pancreatic Enzymes. Crystal Growth & Design. 12: 3594-3602.

495

496   McSweeney, P. L. H. 2004. Biochemistry of cheese ripening. Int. J. Dairy Technol. 57:127–144.

497

498   Ong, L., R. R. Dagastine, S. E. Kentish, and S. L. Gras. 2010. Transmission electron microscopy

499   imaging of the microstructure of milk in cheddar cheese production under different

500   processing conditions. J. Food Sci. 75: 135–145.

501

502   Pellegrino, L. G. Battelli, P. Resmini, P. Ferranti, F. Barone, and F. Addeo. 1997. Effects of heat

503   load gradient occurring in moulding on characterization and ripening of Grana Padano. Lait.

504   77: 217-228.

505

506   Sauer, G. R., W. B. Zunic, J. R. Durig, and R. E. Wuthier. 1994. Fourier transform Raman

507   spectroscopy of synthetic and biological calcium phosphates. Calcif. Tissue Int. 54: 414-

508   420.

509

510   Schrader, K. 2012. Structural analysis of milk and milk products. Strukturanalyse von Milch und

511   Milchprodukten. 133: 30-34.

512

513   Shock, A. A., W. J. Harper, A. M. Swanson, and H. H. Sommer. 1948. What's in those "white

514   specks" on Cheddar. Wisconsin Agric. Experiment. Station. Bull. 474: 31–32.

515

516   Silva, J. V. C., P. D. S. Peixoto, S. Lortal, and J. Floury. 2013. Transport phenomena in a model

517   cheese: the influence of the charge and shape of solutes on diffusion. J. Dairy Sci. 96: 6186–

518   6198.

519

520   Tansman, G., P. S. Kindstedt, and J. M. Hughes. 2014. Powder x-ray diffraction can differentiate

521   between enantiomeric variants of calcium lactate pentahydrate crystal in cheese. J. Dairy

522   Sci. 97: 7354–7362.

523

524   Tansman, G., P. S. Kindstedt, and J. M. Hughes. 2015. Crystal fingerprinting: elucidating the

525   crystals of Cheddar, Parmigiano-Reggiano, Gouda, and soft washed-rind cheeses using

526   powder x-ray diffractometry. Dairy Sci. Technol. 95: 651–664.

527

528   Tlili, M. M., M. Ben Amor, C. Gabrielli, S. Joiret, G. Maurin, and P. Rousseau. 2001.

529   Characterization of CaCO3 hydrates by micro-Raman Spectroscopy. J. Raman Spectrosc.

530   33. 10–16.

531

532   Tuckey, S. L., H. A. Ruehe, and G. L. Clark. 1938. X-ray diffraction analysis of white specks in

533   Cheddar cheese. J. Dairy Sci. 21: 161.

534

535   Washam, C. J., T. J. Kerr, V. J. Hurst, and W. E. Rigsby. 1985. A scanning electron microscopy

536   study of crystalline structures on commercial cheese. Dev. Ind. Microbiol. 26: 749–761.

537   **TABLES**

538   **Table 1**. **Chemical composition of spot, cheese portion around it and whole cheese.***

	MOISTURE	FAT	PROTEIN	ASH
SPOT	$24.2^a \pm 1.2$	$27.5^a \pm 2.6$	$37.6^a \pm 1.3$	$3.9^a \pm 0.1$
CHEESE AROUND THE SPOT	$29.5^b \pm 1.0$	$29.6^a \pm 1.2$	$33.5^b \pm 0.6$	$4.4^b \pm 0.3$
WHOLE CHEESE	$29.8^b \pm 1.0$	$29.9^a \pm 1.1$	$33.5^b \pm 0.2$	$4.4^b \pm 0.2$

539

540   * Data were mean ± standard deviation based on duplicate analyses of five cheeses.

541   [a, b] Means in the same column with different letters are significantly different (p= 0.05).

542

24

543   **FIGURE CAPTIONS**

544   **Figure 1.** Photograph of extra hard cheese showing speaks (SK) and spots (ST). (CS) cheese

545   portion surrounding a spot, sampling mode. Inset, isolated spots from the cheese.

546

547   **Figure 2.** Free amino acid analysis and (inset) light microscopy of a speck isolated from cheese.

548   Bar=200 μm.

549

550   **Figure 3.** Hand-made section of Grana Padano cheese including a spot: light microscopy after

551   ninhydrin staining revealed a dense layer limiting the spot (arrowhead) and the junctions among

552   curd granules (arrows). Bar=200 μm.

553

554   **Figure 4.** Light microscopy of spot semi-thin section (2-5μm) stained with toluidine blue. (a) the

555   curd junctions are visible as darker lines; bar=200 μm. (b): Detail of the large hole in which

556   junctions converge; bar=50 μm. (c) Microcrystals (arrows) along a curd junction; bar=10 μm.

557

558   **Figure 5**. Ultrathin section of spot ultrastructure (a) in comparison with the surrounding cheese (b):

559   the network of electron dense proteins shows a more irregular profile in the spot, particularly at the

560   interface with the electron transparent fat matrix; bar=1 μm.

561

562   **Figure 6**. Free amino acid content of the spot and the cheese portion around it. Data were mean of

563   duplicate analyses of eleven cheeses. (*) Values statistically different ($p<0.05$).

564

565   **Figure 7**. Free amino acid content of the portions 1-3 taken from cheese after the diffusion of 0.3

566   mL aqueous amino acid solution injected in 1 (inset). Data were mean of duplicate analyses.

567

568   **Figure 8.** Calcium phosphate crystals in cheese. (a) Fluorescence microscopy of crystals stained

569   with rodhamine B. (b) Video confocal microscopy of crystals stained with fast green and observed

570   with TRITC and FITC filters, revealing a non-fluorescent core. (c) Ultrathin section of a crystal

571   showing a star shaped zone in the center; at the interface with protein matrix, the fibrillar structure

572   of the crystal is visible (d).

573

574   **Figure 9.** Raman spectrum of calcium phosphate crystal in cheese. Stars represent typical signals of

575   the salt.

576

577   **Figure 10.** Raman spectra (a) and images (b) of spatial distribution of lipid/protein components

578   (red/green areas) around the crystal (covered by the blue area). High, medium and very low

579   component concentrations are indicated as red, green and blue respectively.

580

26

1   **FIGURE CAPTIONS (printed and on-line version)**

2   **Figure 1.** Photograph of extra hard cheese showing speaks (SK) and spots (ST). (CS) cheese

3   portion surrounding a spot, sampling mode. Inset, isolated spots from the cheese.

4

5   **Figure 2.** Free amino acid analysis and (inset) light microscopy of a speck isolated from cheese.

6   Bar=200 µm.

7

8   **Figure 3.** Hand-made section of Grana Padano cheese including a spot: light microscopy after

9   ninhydrin staining revealed a dense layer limiting the spot (arrowhead) and the junctions among

10   curd granules (arrows). Bar=200 µm.

11

12   **Figure 4.** Light microscopy of spot semi-thin section (2-5µm) stained with toluidine blue. (a) the

13   curd junctions are visible as darker lines; bar=200 µm. (b): Detail of the large hole in which

14   junctions converge; bar=50 µm. (c) Microcrystals (arrows) along a curd junction; bar=10 µm.

15

16   **Figure 5**. Ultrathin section of spot ultrastructure (a) in comparison with the surrounding cheese (b):

17   the network of electron dense (grey) proteins shows a more irregular profile in the spot, particularly

18   at the interface with the electron transparent (white) fat matrix; bar=1 µm.

19

20   **Figure 6**. Free amino acid content of the spot and the cheese portion around it. Data were mean of

21   duplicate analyses of eleven cheeses. (*) Values statistically different (p<0.05).

22

23   **Figure 7**. Free amino acid content of the portions 1-3 taken from cheese after the diffusion of 0.3

24   mL aqueous amino acid solution injected in 1 (inset). Data were mean of duplicate analyses.

25

26   **Figure 8.** Calcium phosphate crystals in cheese. (a) Fluorescence microscopy of crystals stained

27   with rodhamine B. (b) Video confocal microscopy of crystals stained with fast green and observed

28   with TRITC and FITC filters, revealing a non-fluorescent core. (c) Ultrathin section of a crystal

29   showing a star shaped zone in the center; at the interface with protein matrix, the fibrillar structure

30   of the crystal is visible (d).

31

32   **Figure 9.** Raman spectrum of calcium phosphate crystal in cheese. Stars represent typical signals of

33   the salt.

34

35   **Figure 10.** Raman spectra (a) and images (b) of spatial distribution of lipid/protein components

36   around the crystal (central dark grey area).

37
38

2
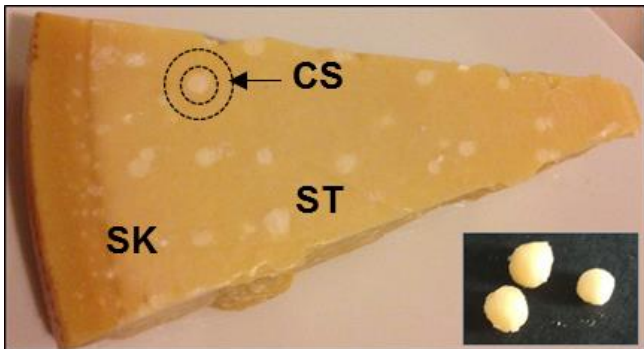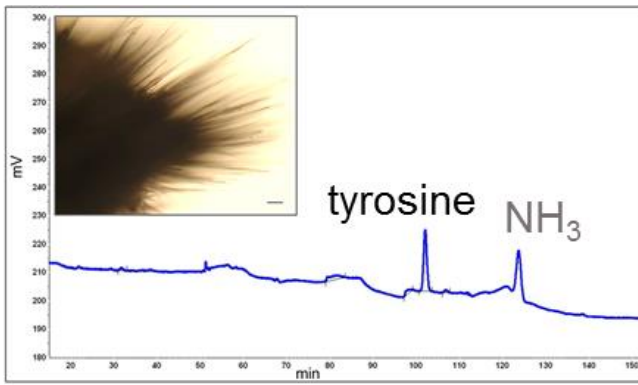
D'Incecco Figure 1.

D'Incecco Figure 2.
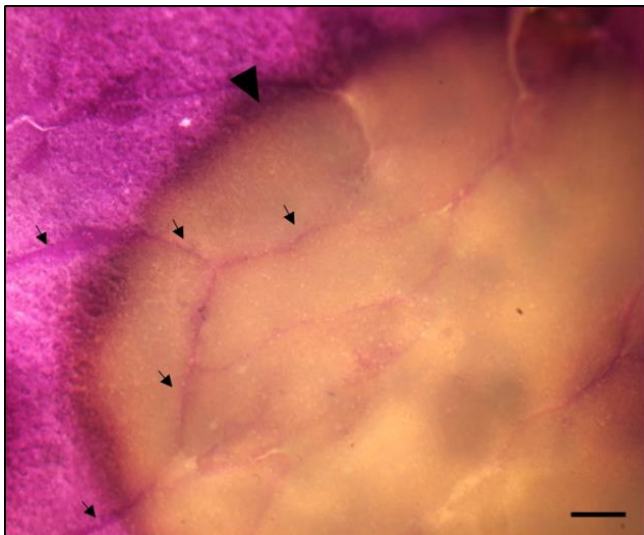
For Peer Review

D'Incecco Figure 3.
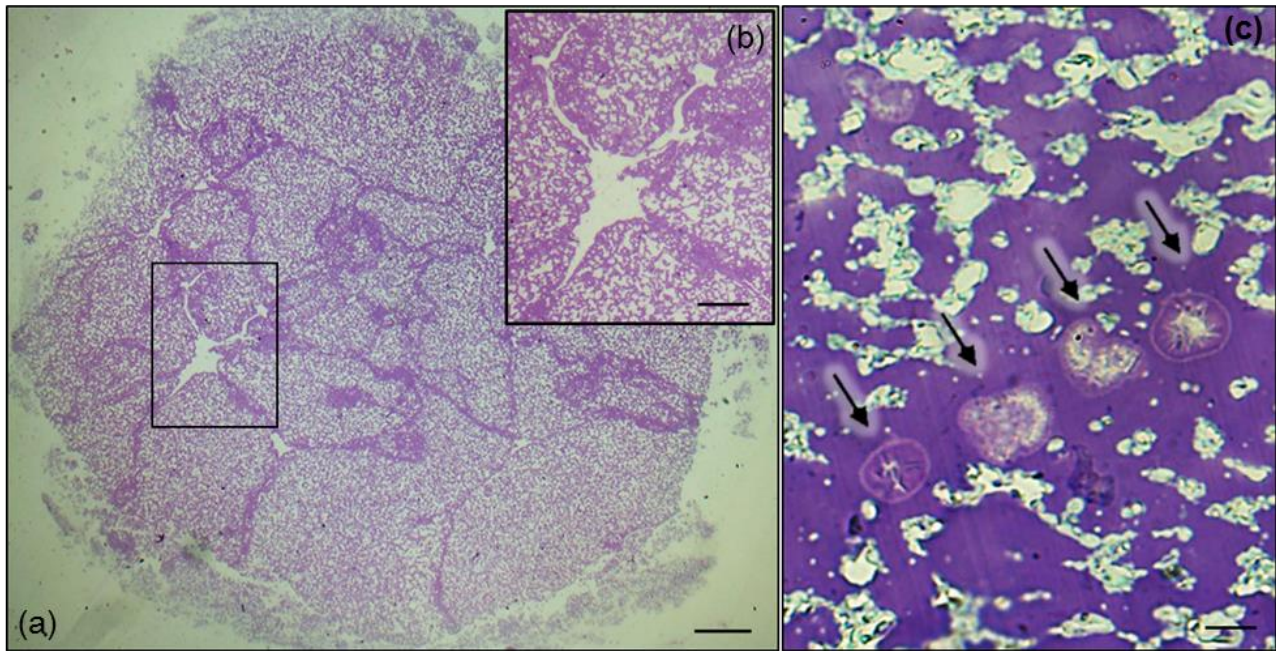
D'Incecco Figure 4.

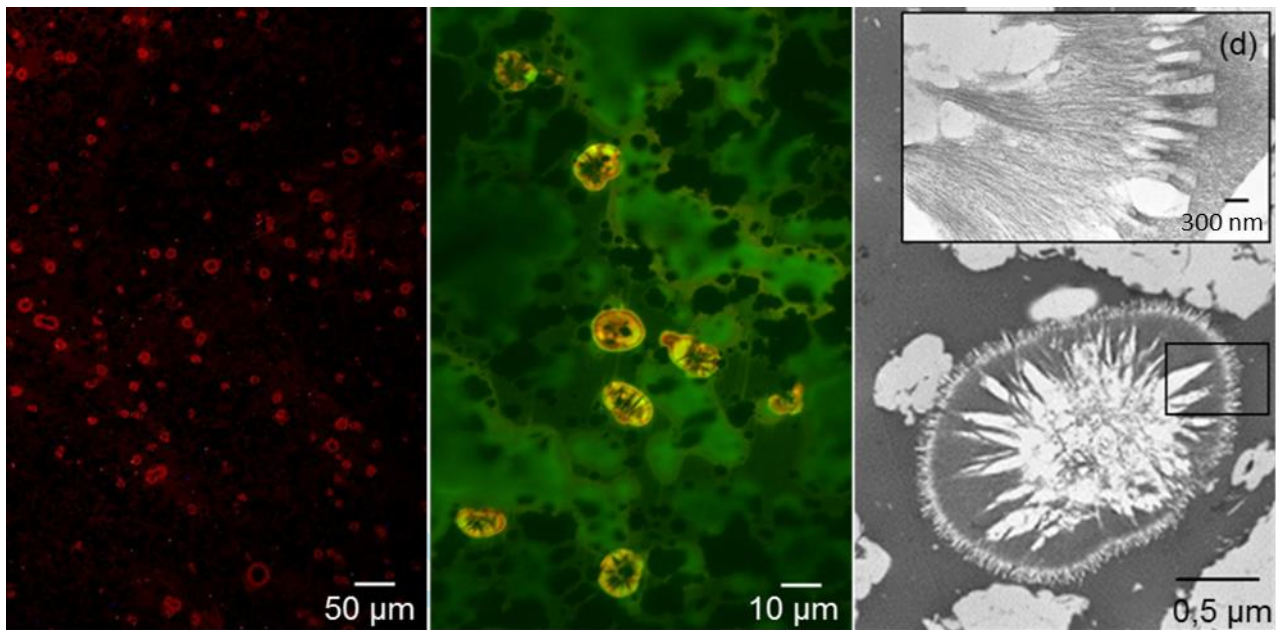**D'Incecco Figure 5**.
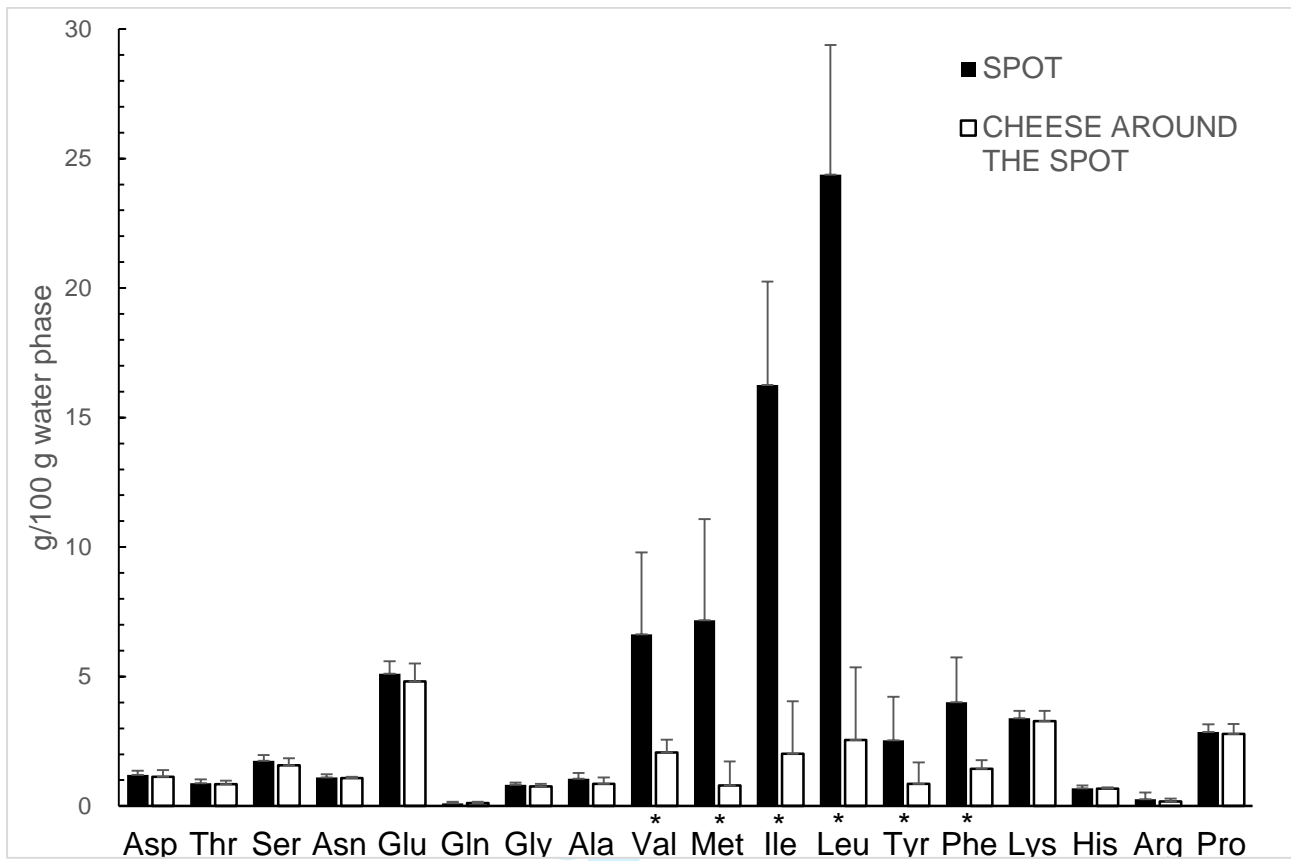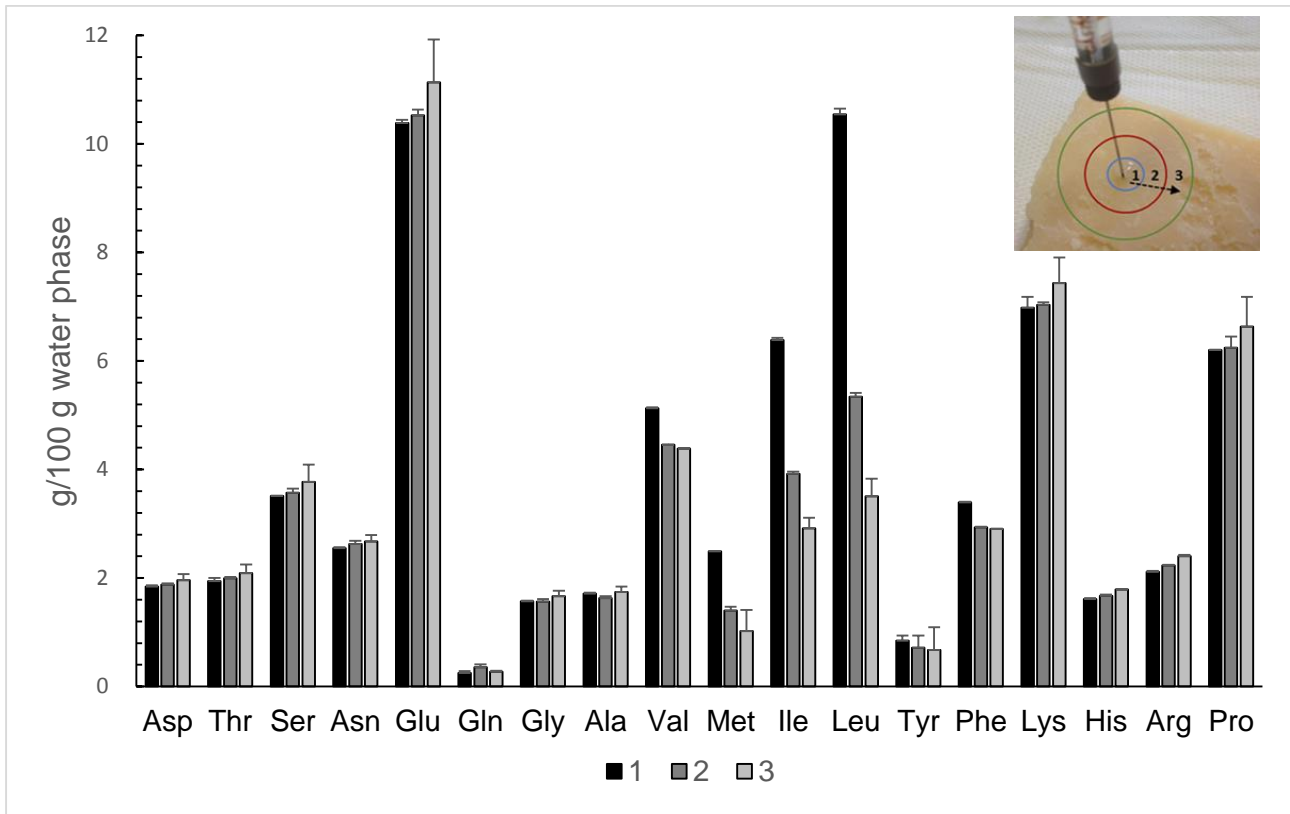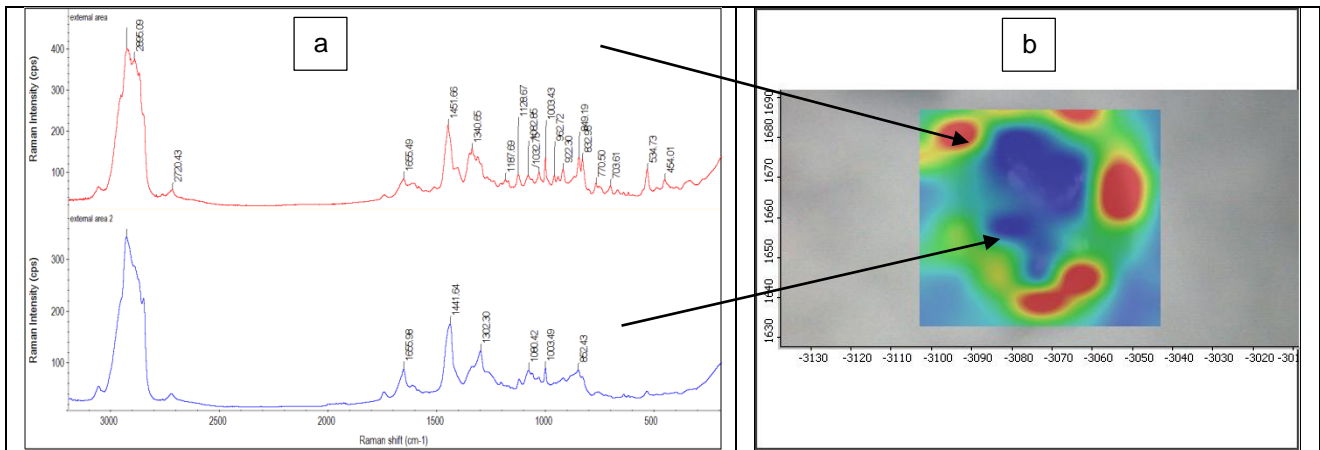
D'Incecco Figure 6.

D'Incecco Figure 7.

D'Incecco Figure 8.
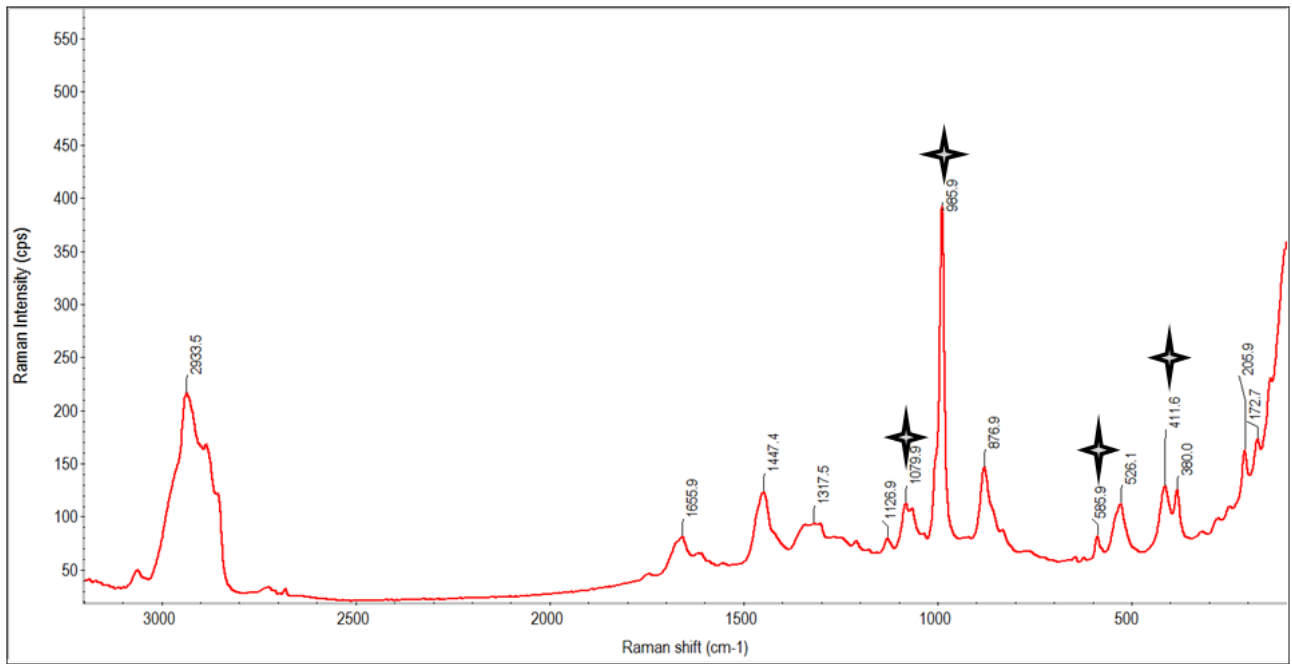
D'Incecco Figure 9.

D'Incecco Figure 10.